Electron-relocalization dynamics in xenon clusters in intense soft-x-ray fields

Mathias Arbeiter, Christian Peltz, and Thomas Fennel*
Universität Rostock, Institut für Physik, Universitätsplatz 3, 18055 Rostock, Germany
(Received 25 February 2014; published 28 April 2014)

Intense and temporally structured x-ray laser fields enable the controlled generation of strongly coupled nonequilibrium cluster nanoplasmas and the time-resolved investigation of their dynamics. Recent femtosecond pump-probe experiments on xenon clusters revealed subpicosecond relaxation dynamics in the cluster nanoplasma via delay-dependent charge states of emitted atomic ions [M. Krikunova *et al.*, J. Phys. B: At. Mol. Opt. Phys. **45**, 105101 (2012)]. Here we report a scheme based on local electron single-particle energy spectra that enables microscopic tracing of the underlying electron-relocalization processes in molecular dynamics simulations up to the strong-coupling regime. We find more efficient recombination in the cluster core and delay-dependent ion charge states, in good agreement with experiments. Our method is applicable to any particle-based plasma simulation and expected to offer insights into correlated relaxation processes in inhomogenous, strongly coupled plasmas.

DOI: 10.1103/PhysRevA.89.043428 PACS number(s): 36.40.Gk, 52.25.Jm, 52.65.Yy

I. INTRODUCTION

Intense laser-cluster interactions in the XUV and x-ray range have become a vibrant area of research due to the rapid development of free-electron laser (FEL) light sources [1–3] and laser-based high-harmonic sources [4,5]. Under intense short-wavelength radiation, atomic clusters transform into dense, transient nanoplasmas that relax and disintegrate on femtosecond to picosecond time scales [6]. The cluster excitation and relaxation dynamics are of topical interest for both the fundamental study of dynamical processes in finite plasmas under short-wavelength light fields [3,7,8] and the development of single-shot diffractive imaging techniques for transient nanoscopic samples [9–13]. XUV pump-probe experiments are emerging as a promising tool for visualizing the underlying processes, as has been analyzed by theory for imaging the ultrafast cluster inner ionization [14].

Cluster dynamics under short-wavelength pulses differs fundamentally from the response to near-infrared (NIR) fields [15,16], where optical field ionization triggers nanoplasma formation [17] and laser energy deposition is dominated by collisional plasma heating and can be greatly enhanced through resonant collective electron excitation and resulting ionization avalanching [18–20]. In XUV and x-ray fields, sequential single-photon ionization of cluster atoms drives the nanoplasma generation [18,21,22] and collisional plasma heating is negligible. As a result, the electron excess energy from the single-photon-induced atomic ionization processes (inner photoemission, Auger cascades) dominates the energy deposition into the nanoplasma via ionization heating [7,23]. Direct consequences are plateaulike electron spectra and efficient electron trapping in the emerging cluster potential [1,24]. In short, the highly nonlinear, field-dominated cluster dynamics at optical frequencies becomes photon dominated in the XUV and x-ray domain, promising the well-controlled generation and precise analysis of relaxation processes in strongly coupled dense nanoplasmas [25].

A striking observation in high-intensity x-ray laser cluster experiments is the exclusive emission of highly charged atomic ions [3]. Though strong x-ray fields efficiently detach electrons from individual atoms and delocalize them in the cluster, measured charge spectra can by no means be explained by laser-induced outer cluster ionization as the efficient Coulomb trapping limits the number of escaping electrons to a tiny fraction. The observed spectra can only be explained by accounting for the subsequent cluster relaxation, where a large fraction of the remaining delocalized cluster electrons first localizes in highly excited, long-living atomic Rydberg states and is then efficiently re-ionized by weak dc electric fields used in ion detection [26]. As a result, final ion charge spectra reflect the ionization stages achieved during laser excitation and their subsequent lowering by recombination of electrons into states below the atomic field-ionization threshold. Strong evidence for the formation of high-lying Rydberg states and their efficient dc field re-ionization has been found in recent velocity-map-imaging experiments using a high-harmonic XUV source [4]. However, the recombination dynamics populating states that recombine permanently is far from being understood but essential for understanding ion spectra. Signatures indicating a pronounced subpicosecond dynamical evolution of recombination processes have been observed in soft-x-ray pump-probe studies on medium-sized xenon clusters at the FLASH free electron laser in Hamburg [27], where average detected ionic charge states were found to increase significantly with pulse delay.

The present work aims at providing a physical picture of the ultrafast relocalization dynamics relevant for understanding the ion charge spectra in laser cluster interactions. We suggest a scheme based on local electron energy spectra to extract and quantify the underlying recombination processes. Our molecular dynamics analysis of soft-x-ray pump-probe excitations of medium sized xenon clusters supports that three-body recombination in the resulting strongly coupled nanoplasma is operational only in the early stages of the subsequent cluster expansion. The microscopic analysis of the resulting charge state lowering by recombination demonstrates a clear shell

*thomas.fennel@uni-rostock.de

 ©2014 American Physical Society

effect with more efficient recombination in the cluster core. The systematic pump-probe analysis shows that recombination is substantially suppressed for long delays and predicts delay-dependent charge states in agreement with corresponding experimental data [27]. Our key conclusions are: (i) Collisional electron relocalization shortly after laser excitation is the main process for understanding the recombination effect to ion spectra; and (ii) time-resolved x-ray laser cluster experiments open a route for the fundamental study of recombination dynamics in strongly coupled plasmas.

II. METHODS

For studying the x-ray laser-cluster interaction we employed a quasiclassical molecular dynamics approach [7,22], where atomic inner shell photoionization and subsequent atomic Auger processes are described via Monte Carlo techniques using experimental cross sections [28–31]. The resulting activated electrons and the ions are propagated classically under a regularized Coulomb interaction and the laser field in dipole approximation. Binary van der Waals interactions between atoms and ions are included via a Lennard-Jones potential and electron impact ionization (EII) is treated with Lotz cross sections [32]. We consider Xe_{923} with closed-shell icosahedral structure under pump-probe x-ray excitation at photon energy $\hbar\omega = 92$ eV, individual pulse width of 30 fs, and intensities $I_{\text{pump}} = 1 \times 10^{13}$ W/cm^2 and $I_{\text{probe}} = 2I_{\text{pump}}$. Similar parameters were used in the pump-probe experiments of Ref. [27]. Statistical ensemble averaging of observables over multiple simulations is performed.

The general dynamics of the laser induced strongly coupled cluster nanoplasma is depicted in Fig. 1, showing the average plasma state evolution in the density-temperature (n-T) plane as calculated from the delocalized cluster electrons. The identification of the latter will be motivated later. The pump excitation generates a warm and dense nanoplasma that cools down via expansion cooling in the relaxation phase. Based on the actual cluster relaxation stage after the pump pulse (black), probe excitation generates additional delocalized electrons and leads to further heating. In a simplified picture, the probe pulse deposits a fixed additional amount of thermal energy and induces a fixed relative density increase of the delocalized electrons. As a result, the plasma state reached immediately after probe excitation exhibits a strongly delay-dependent density but a nearly delay-independent temperature (note the scales in Fig. 1).

For a rough estimate of the effect of the plasma conditions on electron recombination we consider the three-body recombination (TBR) rate per ion for a thermalized, weakly coupled, homogenous plasma [33,34]

$$\Gamma_{\text{TBR}} = \alpha\, n^2 T^{-9/2}, \tag{1}$$

where the prefactor α depends on the structure of the considered ion. For a singly charged hydrogenlike ion it has a value of $\alpha = 8.75 \times 10^{-27}$ cm^6 s^{-1} [35]. The n-T dependence predicted for this simplified case via Eq. (1) is indicated in Fig. 1 via isolines of the recombination rate. Comparison with the delay-dependent plasma states reached by the probe pulse and the subsequent relaxation pathways indicates much

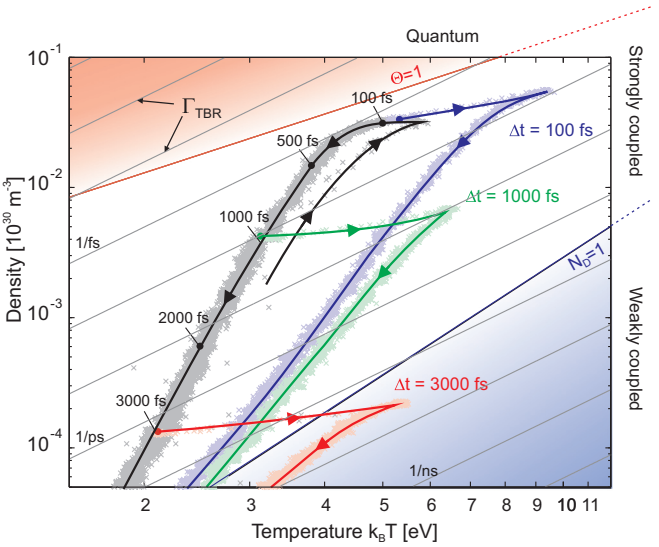

FIG. 1. (Color online) Time-dependent pathways of Xe_{923} in the density-temperature plane for pump (black) and pump-probe excitation (colored, delays as indicated). Crosses show respective snapshots in time, measured relative to the peak of the pump pulse; the temperature T is estimated classically from the mean kinetic energy $k_B T = \frac{2}{3}\langle E_e^{\text{kin}}\rangle$ of delocalized cluster electrons; the density n is derived from the number of delocalized electrons and the cluster radius $R = \sqrt{\frac{5}{3N}\sum_{i=0}^{N} r_i^2}$ with the radial atomic positions r_i. Arrows indicate the evolution and serve as guide to the eyes. Colored areas indicate different plasma regimes, with the degeneracy parameter $\Theta = k_B T/E_F < 1$ (Fermi energy E_F) for the quantum regime (reddish area) and the Debye number $N_D = 4/3\pi n\lambda_D^3 > 1$ (Debye length λ_D) for the weakly coupled regime (bluish area), where $N_D = 1$ corresponds to the plasma coupling parameter $\Gamma = 1/3$ with $\Gamma = \frac{e^2}{4\pi\epsilon_0 k_B T}(\frac{4\pi n}{3})^{1/3}$. Thus the white area illustrates the strongly coupled regime.

lower recombination rates after the probe for longer delays. On the other hand, a higher recombination yield between the pulses is expected in this case, such that additional assumptions would be required for estimating the impacts of these competing effects on the final charge states. However, the simplified analysis shows that (i) the recombination rates realized along the respective pathways change substantially with delay and (ii) the relaxation proceeds predominantly in the regime of strongly coupled, classical (weakly degenerate) plasmas (white area in Fig. 1), justifying a classical molecular dynamics analysis.

III. RESULTS AND DISCUSSION

Starting point for the MD-based recombination analysis is the inner and outer ionization dynamics of the cluster induced by (i) the pump pulse alone and (ii) pump-probe excitation for a short delay of $\Delta t = 100$ fs in Figs. 2(a) and 2(b). Laser-driven atomic photoionization and subsequent Auger and electron impact ionization yield high inner ionization (electrons detached from atomic cores) of $\langle q^i_{\text{inner}}\rangle \approx 4$ and $\langle q^{ii}_{\text{inner}}\rangle \approx 6$, respectively. Outer ionization (excitation of electrons to the continuum) is almost negligible [Fig. 2(a)] due to efficient frustration of outer photoemission by the

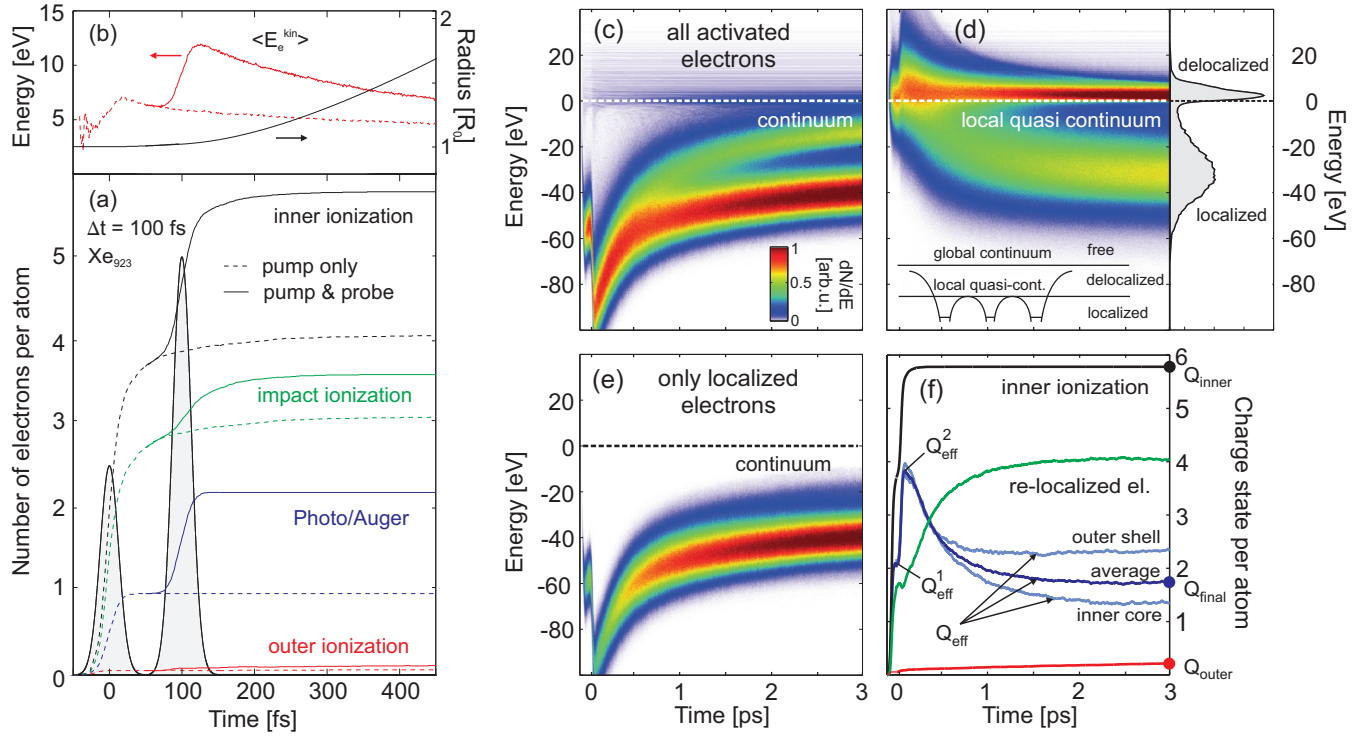

FIG. 2. (Color online) Time-resolved cluster dynamics of a pump-probe excited Xe_{923} with 100 fs delay, $I_{pump} = 1 \times 10^{13}$ W/cm^2 and $I_{probe} = 2I_{pump}$. (a) Ionization dynamics during and shortly after laser excitation; the time axis is centered to the maximum of the pump pulse; dashed lines refer to the pump-only scenario. (b) Correlation between the average kinetic energy of delocalized electrons (red line) and the increasing cluster radius. (c)–(e) Nanoplasma dynamics in terms of single-particle energy spectra of the electrons with respect to either the continuum threshold [(c) and (e)] or the local quasicontinuum [(d)], see text for details. The evolution of the relocalization as well as the main ionization parameters Q_{inner}, Q_{outer}, and Q_{eff} are displayed in (f) together with a shell-resolved analysis of the latter. Solid symbols at $t = 3$ ps indicate converged values, used for the delay-dependent analysis in Fig. 3.

cluster potential. Note that the inner ionization is completed shortly after laser excitation. Ion expansion and the resulting expansion cooling of delocalized cluster electrons begin on the 100 fs time scale [Fig. 2(b)], where the latter effect quickly suppresses thermal electron evaporation from the nanoplasma [7].

A. Electron relocalization analysis

The effect of ionization and expansion on the cluster potential and the resulting nanoplasma dynamics is analyzed in Fig. 2(c) in terms of single-particle energy spectra of the electrons. The continuum threshold clearly distinguishes the free electrons with $E_{sp} > 0$ from the nanoplasma electrons with $E_{sp} < 0$, where the energy distribution of the latter is rapidly shifted downwards with increasing cluster charging. A similar feature was reported for the ionization of Coulomb complexes [21]. Subsequent to this excitation phase, the relaxation phase begins with a highly inner ionized cluster with almost no outer ionization. Departing from an energetically narrow distribution around $E_{sp} \approx -90$ eV after laser excitation, the distribution is continuously shifted to lower binding energies, broadens, and splits into two contributions after about 1 ps. While the first effect visualizes the global cluster potential that becomes shallower under expansion, the remaining features characterize the energetic separation of recombined electrons and remaining delocalized cluster electrons. However, since these global single-particle energy spectra are overlayed by the cluster potential evolution, they do not allow for an unambiguous classification of cluster electrons. To this end, we introduce a local single-particle energy E_{sp}^{loc}. Therefore, the energy is not measured with respect to the continuum threshold but the local quasicontinuum threshold, i.e., the potential barrier between neighboring ions, see inset of Fig. 2(d). Each electron bound to the cluster ($E_{sp} \leqslant 0$) is assigned to the closest ion. The corresponding local barrier V_{loc} is then approximated by the potential in between (halfway) this ion and its nearest neighbor ion, such that the local single-particle energy becomes $E_{sp}^{loc} = E_{sp} - V_{loc}$.

Two main conclusions can be drawn from the evolution of the resulting local single-particle energy spectra in Fig. 2(d), which are now effectively free from the spurious effect of the cluster potential. First, we find a rapid formation of a feature from localized electrons peaked around $E_{sp}^{loc} = -30$ eV. Because of the high local binding energy, this contribution is assumed to reflect the permanently recombined electrons. Second, a strong additional feature from electrons with energies slightly above the local continuum threshold is found, which we denote as delocalized cluster electrons. The fact that their energy distribution narrows continuously is attributed to further expansion cooling as these electrons remain mobile within the cluster. These delocalized electrons

can be efficiently removed (re-ionized) from the cluster after sufficient expansion by external dc detector fields. As these two contributions are energetically well separated, we define all electrons with $E_{\rm sp}^{\rm loc} < 0$ as relocalized [see bimodal distribution in the line plot of the spectrum at $t = 3$ ps in the right panel in Fig. 2(d)]. Based on this criterion, the meaning of the bimodal distribution in the global single-particle energy spectra can be reanalyzed. Comparison of global spectra including only localized electrons [Fig. 2(e)] with the full result spectra [Fig. 2(c)] substantiates that the low-energy feature corresponds to the recombined electrons. Subtracting the number of relocalized electrons from inner ionization leads to an effective charge state, whose asymptotic value we interpret as the final charge state $Q_{\rm final}$ measured in an experiment.

The evolution of relocalization (green) and the resulting effective ion charge states (blue) in Fig. 2(f) show rapid convergence and support average final charge states much higher than the laser-induced cluster outer ionization. As our analysis is of microscopic nature and can be applied to each ionic cell, it allows a spatially resolved analysis of recombination, i.e., as function of the ion position in the cluster. A comparison of ions from the outermost icosahedral shell and ions from the remaining cluster core reveals much higher effective charge states on the cluster surface [cf. light blue lines in Fig. 2(f)]. This result, in turn, indicates more efficient recombination in the core, in agreement with experimental findings [36,37].

B. Pump probe dynamics

For the remaining analysis of the pump-probe effects we first focus on only three key observables, i.e., final effective charge state, inner ionization, and outer ionization, each sampled 3 ps after the probe pulse as indicated by solid symbols in Fig. 2(f) for this particular case.

The following trends are found in the pump-probe dynamics of these observables, see Fig. 3. First, inner ionization (black circles) decreases with increasing delay up to $\approx$1 ps and then remains nearly constant. This effect is attributed to EII driven by electrons created by the probe pulse, which is only efficient at high density, i.e., for short delays. Second, outer ionization increases with delay (red crosses), which can be explained by less efficient trapping of photoelectrons by the cluster potential in later stages of the expansion. However, the values of inner (outer) ionization are much higher (lower) than the typical charge states of about two observed in corresponding experiments [27]. Such values as well as the experimentally observed increase with delay are in agreement with the final charge state $Q_{\rm final}$ predicted by our recombination analysis, see blue squares in Fig. 3.

The comparison of $Q_{\rm inner}$, $Q_{\rm outer}$, and $Q_{\rm final}$ shows less efficient recombination for longer delays. Since recombination proceeds differently before and after the probe pulse, these two stages have to be analyzed separately for extracting a meaningful physical interpretation. The respective contributions can be quantified based on the effective charge states just before ($Q_{\rm eff}^1$) and right after the probe pulse ($Q_{\rm eff}^2$), as depicted in the inset of Fig. 3 showing the time evolution for $\Delta t = 0.5$ ps. The decay of $Q_{\rm eff}^1$ with increasing delay reflects that recombination

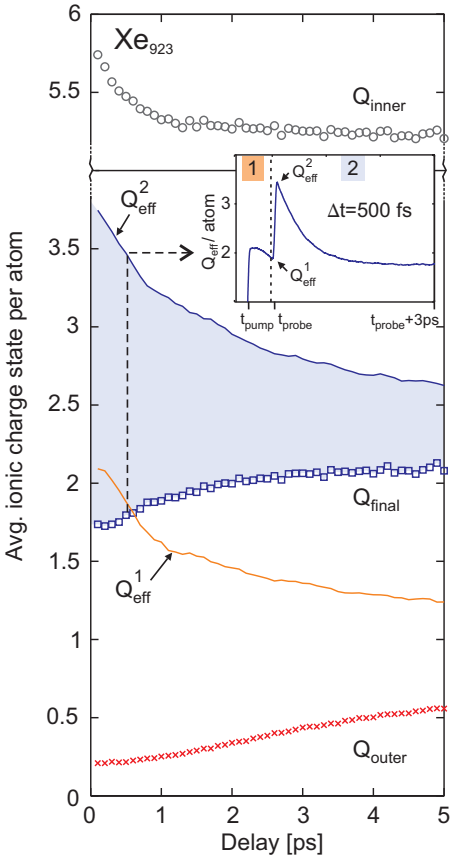

FIG. 3. (Color online) Delay dependence of inner, outer, and effective charge states, evaluated 3 ps after the probe pulse [see solid symbols in Fig. 2(f)]. $Q_{\rm eff}^1$ and $Q_{\rm eff}^2$ denote the effective charge states before and right after the probe pulse. The bluish area illustrates relocalization after probe excitation. Note that $Q_{\rm eff}^1$ is not fully saturated due to the slower cluster expansion.

in between the pulses proceeds for a longer period of time. The subsequent increase of the effective charge states from $Q_{\rm eff}^1$ to $Q_{\rm eff}^2$ by the probe pulse is nearly delay independent. Hence, $Q_{\rm eff}^2$, which is the initial condition for the final relaxation phase, still reflects the recombination between the pulses with higher values for short delays. As the main result of our analysis, the recombination dynamics in the final relaxation phase (after the probe pulse) reverses this trend such that the final charge states are lower for short delays (cf. bluish area in Fig. 3). The general behavior within the two recombination phases is in full agreement with the trends predicted by Fig. 1. The quantitative microscopic analysis shows that the relocalization after the probe pulse is the dominant contribution for sufficiently strong probe excitation.

IV. CONCLUSION

In conclusion, our analysis of recombination dynamics in pump-probe cluster excitations shows competing contributions from the major relaxation phases, i.e., between the pulses and after the probe pulse. As a result the respective contributions have to be taken into account for a quantitative description of ion charge states. For the medium-sized xenon clusters

analyzed here, the magnitude and pump-probe dynamics are in agreement with experiments. The microscopic recombination analysis on the basis of the local single-particle energy spectra reveals more efficient recombination in the cluster core and is able to account for arbitrarily shaped and inhomogeneous targets. We expect that our method is applicable to laser ionized nanoplasmas in general, irrespective of excitation wavelength and provides a valuable tool for analyzing recombination processes in laser-driven nanosystems. The relocalization dynamics itself is of particular interest for x-ray imaging experiments, as only localized electrons contribute to the scattering that contains information on the atomic structure.

ACKNOWLEDGMENTS

Financial support from the Deutsche Forschungsgemeinschaft within SFB 652/3 and computer time provided by the HLRN Computing Center are gratefully acknowledged.

[1] C. Bostedt *et al.*, Phys. Rev. Lett. **100**, 133401 (2008).
[2] H. Thomas *et al.*, Phys. Rev. Lett. **108**, 133401 (2012).
[3] T. Gorkhover *et al.*, Phys. Rev. Lett. **108**, 245005 (2012).
[4] B. Schütte, M. Arbeiter, Th. Fennel, M. J. J. Vrakking, and A. Rouzée, Phys. Rev. Lett. **112**, 073003 (2014).
[5] B. F. Murphy, K. Hoffmann, A. Belolipetski, J. Keto, and T. Ditmire, Phys. Rev. Lett. **101**, 203401 (2008).
[6] H. Wabnitz *et al.*, Nature (London) **420**, 482 (2002).
[7] M. Arbeiter and T. Fennel, Phys. Rev. A **82**, 013201 (2010).
[8] U. Zastrau *et al.*, Phys. Rev. Lett. **112**, 105002 (2014).
[9] R. Neutze, R. Wouts, D. van der Spoel, E. Weckert, and J. Hajdu, Nature (London) **406**, 752 (2000).
[10] H. N. Chapman *et al.*, Nature (London) **448**, 676 (2007).
[11] H. N. Chapman *et al.*, Nat. Phys. **2**, 839 (2006).
[12] C. Bostedt *et al.*, Phys. Rev. Lett. **108**, 093401 (2012).
[13] D. Rupp *et al.*, New J. Phys. **14**, 055016 (2012).
[14] I. Georgescu, U. Saalmann, and J. M. Rost, Phys. Rev. Lett. **99**, 183002 (2007).
[15] T. Fennel, K.-H. Meiwes-Broer, J. Tiggesbäumker, P.-G. Reinhard, P. M. Dinh, and E. Suraud, Rev. Mod. Phys. **82**, 1793 (2010).
[16] U. Saalmann, C. Siedschlag, and J. M. Rost, J. Phys. B: At. Mol. Opt. Phys. **39**, R39 (2006).
[17] T. Ditmire, Phys. Rev. E **54**, 6735 (1996).
[18] U. Saalmann and J. M. Rost, Phys. Rev. Lett. **91**, 223401 (2003).
[19] J. Zweiback, T. Ditmire, and M. D. Perry, Phys. Rev. A **59**, R3166 (1999).
[20] T. Fennel, T. Döppner, J. Passig, C. Schaal, J. Tiggesbäumker, and K.-H. Meiwes-Broer, Phys. Rev. Lett. **98**, 143401 (2007).
[21] C. Gnodtke, U. Saalmann, and J. M. Rost, New J. Phys. **13**, 013028 (2011).
[22] I. Georgescu, U. Saalmann, and J. M. Rost, Phys. Rev. A **76**, 043203 (2007).
[23] M. Arbeiter and T. Fennel, New J. Phys. **13**, 053022 (2011).
[24] Y. Ovcharenko *et al.*, Phys. Rev. Lett. **112**, 073401 (2014).
[25] L. Ramunno, C. Jungreuthmayer, and T. Brabec, Laser Phys. **17**, 618 (2007).
[26] T. Fennel, L. Ramunno, and T. Brabec, Phys. Rev. Lett. **99**, 233401 (2007).
[27] M. Krikunova *et al.*, J. Phys. B: At. Mol. Opt. Phys. **45**, 105101 (2012).
[28] A. Aguilar, J. D. Gillaspy, G. F. Gribakin, R. A. Phaneuf, M. F. Gharaibeh, M. G. Kozlov, J. D. Bozek, and A. L. D. Kilcoyne, Phys. Rev. A **73**, 032717 (2006).
[29] E. D. Emmons, A. Aguilar, M. F. Gharaibeh, S. W. J. Scully, R. A. Phaneuf, A. L. D. Kilcoyne, A. S. Schlachter, I. Álvarez, C. Cisneros, and G. Hinojosa, Phys. Rev. A **71**, 042704 (2005).
[30] P. Andersen, T. Andersen, F. Folkmann, V. K. Ivanov, H. Kjeldsen, and J. B. West, J. Phys. B: At. Mol. Opt. Phys. **34**, 2009 (2001).
[31] U. Becker and D. A. Shirley, *VUV and Soft X-Ray Photoionization* (Springer, New York, 1996).
[32] W. Lotz, Z. Phys. **206**, 205 (1967).
[33] E. Ackad, N. Bigaouette, S. Mack, K. Popov, and L. Ramunno, New J. Phys. **15**, 053047 (2013).
[34] Y. Hahn, Phys. Lett. A **231**, 82 (1997).
[35] J. D. Huba, *NRL Plasma Formulary* (Naval Research Laboratory, Washington, DC, 2009), pp. 54–55.
[36] M. Hoener, C. Bostedt, H. Thomas, L. Landt, E. Eremina, H. Wabnitz, T. Laarmann, R. Treusch, A. R. B. de Castro, and T. Möller, J. Phys. B: At. Mol. Opt. Phys. **41**, 181001 (2008).
[37] H. Thomas, C. Bostedt, M. Hoener, E. Eremina, H. Wabnitz, T. Laarmann, E. Plönjes, R. Treusch, A. R. B. de Castro, and T. Möller, J. Phys. B: At. Mol. Opt. Phys. **42**, 134018 (2009).